Anharmonicity effects in the frictionlike mode of graphite

C. Menéndez,[1] A. Lobato,[2] D. Abbasi-Pérez,[3] J. Fernández-Núñez,[4] V. G. Baonza,[2] and J. M. Recio[1,*]
[1]*MALTA-Consolider Team and Departamento de Química Física y Analítica, Universidad de Oviedo, E-33006 Oviedo, Spain*
[2]*MALTA-Consolider Team and Departamento de Química Física I, Universidad Complutense de Madrid, E-28040 Madrid, Spain*
[3]*King's College London, London, WC2R 2LS, United Kingdom*
[4]*Departamento de Física, Universidad de Oviedo, E-33006 Oviedo, Spain*
(Received 30 November 2015; revised manuscript received 19 March 2016; published 13 April 2016)

Graphite is a prototypical solid lubricant demanding a thorough understanding of its low-friction behavior. The $E_{2g}(1)$ Raman active vibrational mode of graphite is associated with the rigid-layer relative movement of its graphene sheets. Thus, this mode can provide a good means of exploring the low resistance of graphene layers to slip with respect to each other. To take advantage of this fact, the anharmonicity of the $E_{2g}(1)$ mode has to be carefully characterized and evaluated since the atomic arrangement of carbon atoms in the ambient condition ABA stacking of graphite evidences potential asymmetry. The calculated one-dimensional energetic profile of the $E_{2g}(1)$ mode reveals this local anisotropy around the energy minima and can be microscopically interpreted in terms of electron density interactions. Morse-type potentials accurately fit the energetic profiles at different interlayer separations, and provide simple analytical expressions for evaluating harmonic and anharmonic contributions to the Γ-point $E_{2g}(1)$ frequency $\omega_{E_{2g}(1)}$ under a perturbative algebraic treatment. We quantify how the anharmonic contribution increases with the available energy (E) at zero pressure, and how this contribution decreases as hydrostatic pressure (p) or uniaxial stress is applied for a given available energy. The calculated $\omega_{E_{2g}(1)} - p$ and $\omega_{E_{2g}(1)} - E$ trends indicate an increasing (decreasing) of frictional forces in graphite with pressure (temperature). Our conclusions are supported by the good agreement of the calculated frequencies with existing Raman experiments under hydrostatic pressure conditions.

DOI: 10.1103/PhysRevB.93.144112

I. INTRODUCTION

Graphite is among the best solid lubricants, but it is also known that graphite behaves as a poor lubricant in vacuum [1]. Such a diverse behavior makes graphite a target model in many frictional/tribological studies at both macroscopic [2] and atomic [3–5] levels. Graphite also was the first system studied in the seminal work by Mate *et al.* [6], when the friction force microscope was developed. Nowadays, graphene has emerged into the scene of frictional studies [7–9] and many works have been focused on understanding the underlying mechanisms of friction in graphite [10,11] and graphene [12]. For instance, novel terms such as superlubricity [13,14] have been coined to refer to the near-zero friction force observed between a graphite substrate and a graphite flake in an incommensurate configuration.

The vibrational $E_{2g}(1)$ mode of graphite describes a rigid-layer relative movement of the graphene sheets (see Fig. 1), thus informing on the forces that graphene layers have to overcome in order to initiate relative displacements [15,16]. By means of the characterization of this vibrational mode and the evaluation of the energetic profile accompanying its atomic movements, it is possible to get insight into the corrugation energy landscape and the frictional behavior of graphite at a microscopic level. One of the relevant points at this regard is to accurately take into account the anharmonicity of this Raman active mode. It is expected to be noticeable, leading to a stress-induced blue-shift of its frequency greater than in other IR and Raman higher-frequency modes [17,18]. This vibrational mode may be also used to verify the presence of graphene among graphitelike samples containing few layers graphene. Although present in graphite and absent in graphene, the Raman active $E_{2g}(1)$ mode "cannot be (directly) used as method for an experimental verification of graphene" [19] due to its low Raman intensity [20]. However, since the frequency of this mode is a measure of the splitting experienced by the E_{2g} mode in graphene into the infrared active E_{1u} and the Raman active $E_{2g}(2)$ modes of graphite [21], the lower frequency of this $E_{2g}(2)$ mode in graphite with respect to graphene could be used as a potential way to discriminate between graphite and graphene, albeit this is a matter of current controversy [22].

From a more theoretical perspective, it should be noticed that in the $E_{2g}(1)$ mode, the in-plane and out-of-phase atomic movements (see Fig. 1) yield negligible modifications in the intralayer C-C network. The frequency of this shearlike mode was observed below 50 cm^{-1} at ambient conditions (see, for example, Refs. [21,23,24] and references therein) and provides a direct and accurate manifestation of the weak van der Waals (vdW) interactions between graphene sheets in graphite. This is a relevant issue that deserves some comments since the interplay between vibrational modes and vdW and covalent interactions in graphite has aroused interest with detailed analysis for decades. In the pioneer works of Dresselhaus *et al.* [21,23] and the more recent studies of Cousins *et al.* [24], the focus was on the simultaneous modelization of both types of interactions (also introducing anharmonic contributions) to account for experimental elastic data and Γ-point vibrational frequencies. As highlighted in these works, difficulties in the parametrization of C interactions appear not only due to the coexistence of both strong and weak interactions but for the fact that the former are well localized and the later are of a nondirectional type. Clearly, a theoretical determination of the energy profile involved in the $E_{2g}(1)$ mode would

*Corresponding author: jmrecio@uniovi.es

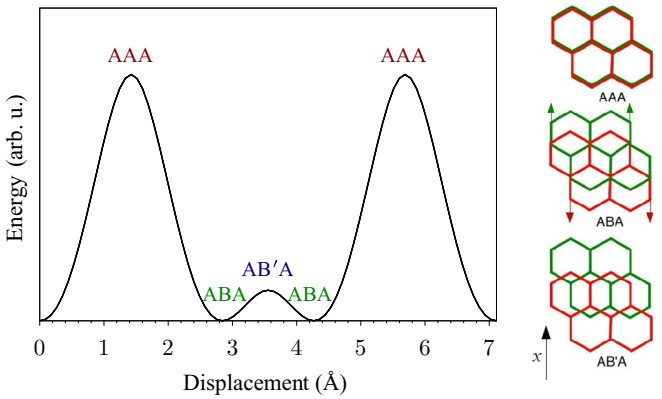

FIG. 1. On the left, energetic profile versus the relative displacement of the middle layer of the ABA equilibrium configuration for a given interlayer distance along a selected direction (the x direction). On the right, arrangements of the trilayer slab associated with graphite stackings at critical points. C atoms in the central layer B are in green. C atoms in A layers are in red. Arrows indicate the atomic movements involved in the $E_{2g}(1)$ vibrational mode.

benefit an unambiguous characterization of vdW interactions in graphite-based materials.

By performing detailed first-principles calculations, it is possible to accurately describe the simultaneous energetics involved in intralayer and interlayer C-C interactions. Among the number of computational simulations related to this topic, and in the context of our study, it is worth mentioning the early works of di Vincenzo *et al.* [17] [with explicit reference to anharmonicity in the $E_{2g}(1)$ mode] and Gonze *et al.* [25], where the lack of an accurate computational methodology was discussed. More recently, vdW contributions were specifically taken into account in the calculations [15,16,26–29], and the particular energetic barrier involved in the transition from the stable ABA to the AAA stacking of graphene sheets in graphite was calculated [15,16,26,27]. From the energetic profiles connecting both stackings, the vibrational frequency of the $E_{2g}(1)$ mode can be straightforwardly calculated [16]. Anharmonicity of phonons in carbon-based materials has also been the subject of rigorous theoretical studies by Bonini *et al.* [22] and Paulatto *et al.* [30] (and references therein). In these works, the focus is on the phonon scattering mechanisms and the characterization of phonon decays [22] with the aim at determining thermal transport properties of these materials [30], though neither explicit nor implicit reference to friction phenomena was reported.

Fortunately, an extensive experimental work [18], including effects of hydrostatic pressure on this frequency, provides a pertinent source of information to compare with these computational studies. Moreover, from the frequency (ω) and pressure (p) experimental data of Hanfland *et al.* [18], linear Grüneisen parameters were derived, thus allowing for a comprehensive discussion of anharmonicity in the $E_{2g}(1)$ mode.

Taking into account the above considerations, we pursue in this investigation to provide a thorough understanding of anharmonicity in the $E_{2g}(1)$ mode of graphite by rendering, modeling, and evaluating this vibrational mode under different stress conditions. By rendering we mean an illustrative description of the atomic arrangements with specific attention to the local anisotropy around the absolute energy minima, and an interpretation of the surface energy potential landscape using intuitive images of charge density interactions. A simple four-spring model and a perturbative treatment using Morse-type functions are enough to reasonably account for the anharmonicity associated to this mode. The evaluation stage consists in a detailed analysis of part of our previous DFT-based calculations in graphite under different stress conditions [16]. Specifically, we examined the results of a three-layer graphene slab in which the middle layer is forced to slide between two other ones, which remain fixed at different interlayer distances, thus mimicking the atomic movements involved in the $E_{2g}(1)$ mode [16]. Morse functions accurately account for energy changes along the vibrational coordinate of this mode at different interlayer separations. It will be shown that anharmonicity decreases as this parameter decreases or, equivalently, hydrostatic pressure or uniaxial stress is applied. Overall, our calculations provide a quantitative assessment of the anharmonic contribution of this rigid-layer frequency mode of graphite under different strain scenarios, and inform on the trends that frictional forces show as temperature increases and pressure is applied.

The rest of the paper is divided in four more sections. In the next one, we present geometrical and energetic proofs to show that the $E_{2g}(1)$ mode must evidence anharmonicity. In Sec. III, we introduce a simple four-spring model along with the algebraic treatment of anharmonicity and its dependence on stress. In Sec. IV, harmonic and anharmonic calculated results are analyzed at zero pressure and up to 14 GPa, including explicit comparison with available experimental data in the same pressure range. The paper ends with the main conclusions of our work.

II. PROOFS OF ANHARMONICITY FROM ATOMIC ARRANGEMENTS AND ENERGETIC CONSIDERATIONS

To start with, we look at Fig. 1 just to visualize the three different stackings distinguished at the right which are pertinent for the analysis of the $E_{2g}(1)$ mode. The two symmetric minima are equivalent and exemplify the equilibrium ABA stacking, in which half of the atoms of layers B share the z axis with half of the atoms of layers A. The z axis is the one perpendicular to the graphene layers. By displacing the middle graphene layer from the ABA configuration (first minimum at around 2.8 Å) along one side of the x axis we reach the highest-energy configuration, the AAA stacking. On the other hand, when the B layer is shifted to the other side of the x axis, a third stacking labeled AB′A and associated with the low-energy maximum is found. In this AB′A configuration there is not any single C atom in layers B above or below any C atom in layers A. Although at first sight the periodicity of the structure might induce to think otherwise, the existence of these two different energy profiles around the equilibrium ABA configuration forces the $E_{2g}(1)$ mode to follow a strong anharmonic conduct. This is one key point for understanding the anharmonicity of this frictional-like mode of graphite.

The two panels of Fig. 2 should be used in order to gain a further insight of the main repulsive electrostatic interactions involved in the energy profile displayed in Fig. 1. Although

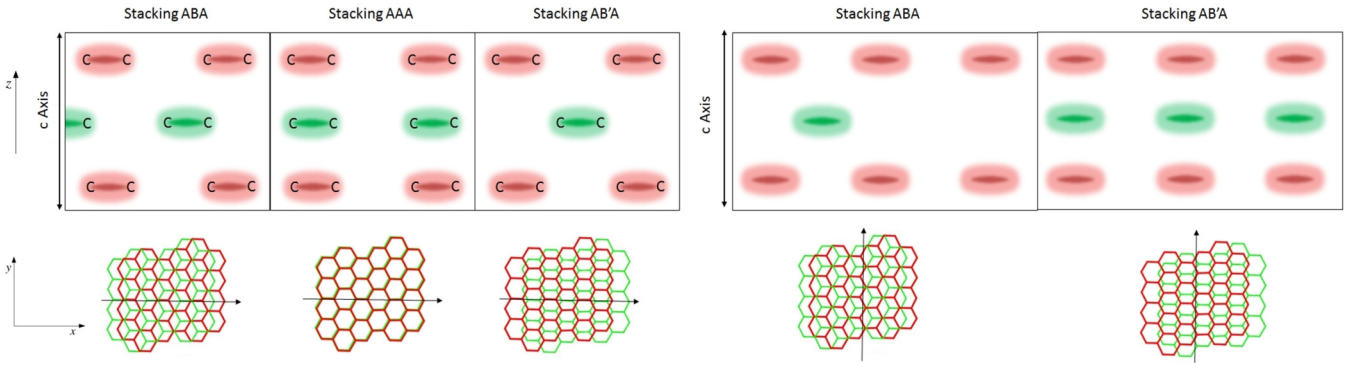

FIG. 2. Schematic representation of the bonding charge densities and interaction patterns for different graphite stackings (see text) along the z axis. Left panel: frontal (sliding) view, along the x axis, as indicated by the arrow. Right panel: side view, along the y axis, as indicated by the arrow.

it only gathers a schematic representation of the positions of atoms and bond charge densities perpendicular to the graphene planes (see Ref. [25] for some true computed and experimental maps), this figure contains the basic information to interpret the relative energetic order of the three atomic configurations. In the left panel, we have inspected the frontal view along the x axis for these three stackings. As expected, the AAA stacking shows the highest number of repulsive interactions between C-C intralayer bonds of different layers. In this AAA configuration, the repulsions are more effective because both atoms and bonds are on top of each other. In contrast, there is not any clear reason in this picture which explains why ABA is less energetic than AB′A. However, if we consider the interactions along the y axis (side view) in the second panel then a justification can be given. Realizing that the chosen axis does not cross any C atom in any layer, in the AB′A stacking the C-C bonds are overlayed displaying a bridelike arrangement with C-C bond densities always on top of each other. In contrast, in the ABA stacking the bonds never overlay each other, and only one bond in layer B is crossed for every three bonds in layer A. Since the ABA stacking shows the less number of interlayer repulsive interactions, this simple picture provides an explanation to understand the preference of graphite for the ABA stacking in agreement with the energetic profile of Fig. 1.

To quantify the energy changes along the normal coordinate of the $E_{2g}(1)$ mode, we briefly recall to our recent first-principles total-energy calculations for a trilayer graphene (3LG) [16]. 3LG is a periodic slab model of three graphene layers in an initial ABA stacking representing the Bernal-type configuration of stable bulk graphite. The calculations were performed within the density-functional theory (DFT) formalism with a plane-wave pseudopotential approach using the Perdew-Burke-Ernzerhof (PBE) generalized gradient exchange-correlation functional [31] as implemented in the VASP code [32]. We followed the standard projector augmented wave all-electron description of the electron-ion-core interaction. Brillouin-zone integrals were also approximated using the Monkhorst-Pack method [33], and the energies converged to 1 meV with respect to k-point density ($16 \times 16 \times 8$ k meshes) and the plane-wave cutoff (600 eV). Grimme's correction [34] was included to account for dispersion interactions. In our previous work [16], it was noticed that Grimme-D2 correction tends to overestimate the weak dispersion forces between graphite layers (see also Rêgo *et al.* [29]) yielding a calculated c lattice parameter (6.43 Å) slightly lower than the experimental value (6.70 Å). Nevertheless, an overall agreement with the experimental data was found as also discussed by Bucko *et al.* [35].

We simulated the atomic movements by fixing the atoms of the A layers, and displacing the B layer along the x direction a number of different distances away from its equilibrium position up to the next equivalent ABA stacking, relaxing the geometry in every point. To prevent the B layer to reach again the initial minimum of the potential energy surface after the geometry optimization, we fixed the x and y coordinates of one of the C atoms of the B layer, leaving its z coordinate and the coordinates of the unconstrained C atom (and therefore the C-C distance) as free parameters in the relaxation process. As a first result, we found no differences between the bond length (1.42 Å) of bulk graphite and the 3LG slab model at the bulk interlayer equilibrium distance. In order to include the structures AB′A, AAA, and the specular image of the initial ABA stacking in the sliding path, we used the TETR code [36] to displace the B layer 48 points in steps of 0.0889 Å, for a total displacement of 4.2672 Å not only along the normal direction of this frictionlike vibrational mode of symmetry E_{2g} (1), but also for different sliding directions from 0° to 110° in 10° steps. To simulate the effect of hydrostatic pressure or uniaxial stress on the mode, we repeated the process at different fixed interlayer distances, and used our reported equations of state [16].

A series of isomorphous energetic profiles similar to that shown in Fig. 1 were obtained with these computational parameters at selected interlayer spacings decreasing from 3.450 to 2.800 Å [16]. To summarize our previous calculations, we display in Fig. 3 the complete energetic landscape involved in the $E_{2g}(1)$ vibrational mode. Notice that the center of the gray and black regions are associated with the AAA and ABA configurations, respectively, whereas the AB′A stacking appears at the saddle points connecting two adjacent maxima and minima. In this picture, we recover the energetic profile shown in Fig. 1 as we move along the 0–180 direction. The local asymmetry around the ABA minimum at the origin is apparent, thus illustrating the energetic difference as the B layer is displaced either backward or forward from the origin along this direction. On the contrary, as expected from the hexagonal symmetry of the graphene sheet, if we examine the

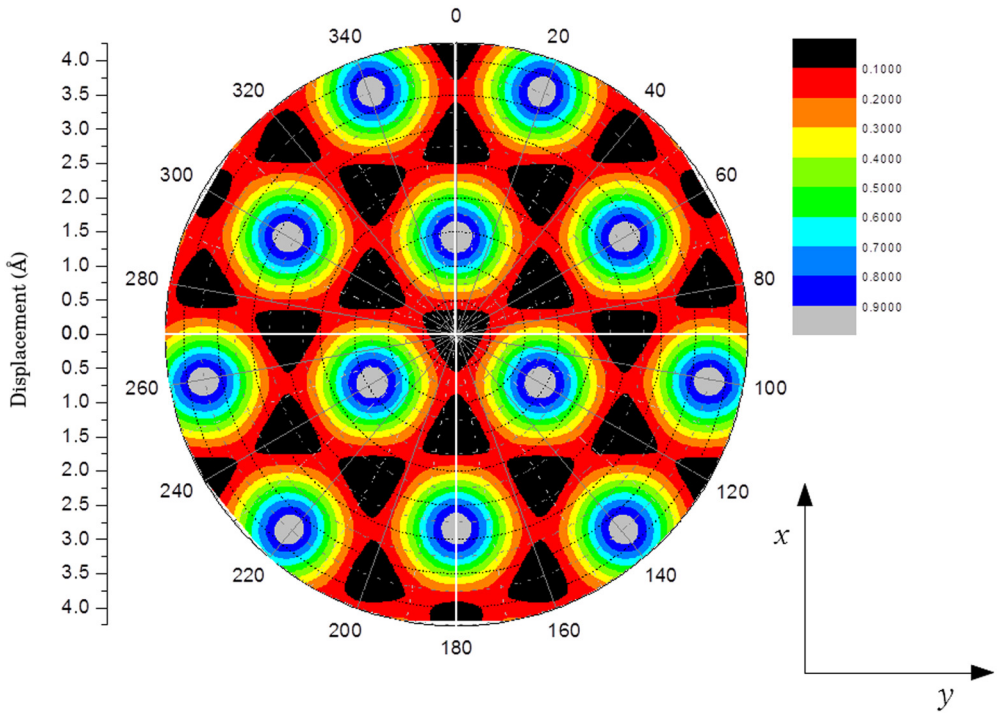

FIG. 3. Polar energy landscape for the $E_{2g}(1)$ mode. A normalized energy scale with a constant energy step is used. White lines stand for 0–180 and 90–270 directions.

90–270 direction we find a totally symmetric energetic profile around the ABA minimum at the origin without finding either the AAA or the AB′A stacking. These two specific directions exemplify the high anisotropy of the energetics involved in the $E_{2g}(1)$ mode, which is also relevant for the analysis of its anharmonicity.

III. MODELING THE ANHARMONICITY OF THE $E_{2g}(1)$ MODE

A rather simple spring model accomplishing the bonding interactions involved in the $E_{2g}(1)$ mode is depicted in Fig. 4.

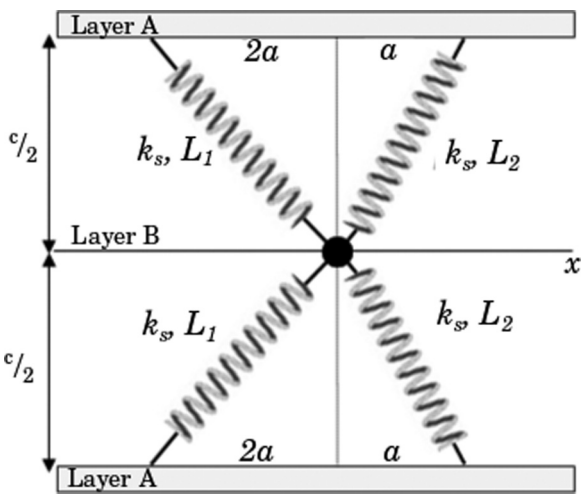

FIG. 4. Scheme of the four-spring model. Symbols are defined in the text.

Similar semiempirical models have been successfully applied to graphite vibrational modes in the past [20]. The model considers four springs attached to a C atom in the middle layer and having the other ends attached to C atoms in the A layers. The four springs have the same value of the constant k_s, and their lengths are equal in pairs. Their natural lengths L_1 and L_2 depend on the interlayer distance $c/2$. The value of a is the C-C bond length ($a = 1.42$ Å under zero stress). By changing the effective length of the springs, we simulate the atomic displacement of the C atoms in the middle layer along the x coordinate under a potential given by the equation

$$V(x) = k_s\big[(\sqrt{(c/2)^2 + (x+2a)^2} - L_1)^2 + (\sqrt{(c/2)^2 + (x-a)^2} - L_2)^2\big], \quad (1)$$

that leads to the following expression for the harmonic frequency (m is the oscillating mass):

$$\omega_H = \sqrt{\frac{V''(0)}{m}}; \quad V''(0) = k_s \frac{8+5e^2}{(1+e^2)(4+e^2)}; \quad e = \frac{c/2}{a}. \quad (2)$$

We will check the validity of the above expression in the next section.

A different approach is understanding anharmonicity in a perturbative fashion. Since the behavior of the real potential curve is slightly different to the harmonic one, a third-order Taylor expansion of the potential suffices for our purposes. A quartic term introduces a smaller and positive correction in the frequency, but here we are only interested in the first-order anharmonicity. Hence, the potential can be simply expressed

as the sum of a quadratic and a cubic term:

$$V(x) = \tfrac{1}{2}kx^2 + \tfrac{1}{2}\alpha x^3. \quad (3)$$

The quadratic term includes information about the second derivative of the potential, and allows us to obtain the value of the harmonic constant k. On the other hand, the cubic term corrects the harmonic potential through the parameter α, related with the third derivative of the real potential.

By means of a perturbative treatment of both the period and the displacements from the equilibrium point of this asymmetric oscillation, it is straightforward to derive an expression for the frequency as a sum of the harmonic frequency (ω_H) and a perturbation (ω') [37]:

$$\omega = \omega_H + \omega', \quad (4)$$

with

$$\omega_H = \sqrt{\frac{k}{m}}; \quad \omega' = -\frac{15}{16}\frac{A^2\alpha^2}{m^2\omega_H^3}. \quad (5)$$

The anharmonic perturbation depends on the available vibrational energy through the harmonic amplitude A, $E = \frac{1}{2}kA^2$, and its harmonic frequency, but also on the value of α and the mass of the system. In the equation above, we see that anharmonicity is always a negative contribution to the actual frequency.

Aiming for a physical interpretation of our results, we used a Morse-type potential V_M, already included in the analysis of di Vincenzo *et al.* [17], to fit the computed data:

$$V_M(x) = V_e + M\left(1 - e^{-N(x-x_e)}\right)^2, \quad (6)$$

where $V_e = V_M(x_e)$ is the potential energy of the system for one carbon atom at the equilibrium ABA configuration of graphite. The main advantage is that the anharmonic contribution can be represented as a function of the available vibrational energy and the parameters of the Morse potential M and N:

$$\omega(E) = \omega_H\left[1 - \frac{15}{16}\frac{E}{M}\right]; \quad \omega_H = N\sqrt{\frac{2M}{m_C}}, \quad (7)$$

being m_C the mass of one single carbon atom.

Our modeling also considers the use of Eqs. (8) and (9), previously employed in the analysis of the experimental data [18]:

$$\frac{\omega(p)}{\omega(0)} = \left[\frac{\delta_0}{\delta'}p + 1\right]^{\delta'}; \quad \delta_0 = \left(\frac{d\ln\omega}{dp}\right)_{p=0};$$
$$\delta' = \left[\frac{d}{dp}\left(\frac{d\ln\omega}{dp}\right)\right]_{p=0}. \quad (8)$$

The relation between frequency and pressure allows us to obtain δ_0 and δ', which are linear analogs to those included in the Murnaghan equation of state, through a least-squares fit. Since the perturbative model provides the anharmonic contribution to the frequency of the $E_{2g}(1)$ mode, Eq. (8) can be used to assess the quality of our computed dependence on pressure of the anharmonicity of this mode by simply comparing calculated and experimental fitting parameters. Furthermore, the pressure dependence of the frequency can also be used to evaluate the linear or one-dimensional Grüneisen parameter $\gamma_\parallel$ through the equation [38]

$$\frac{\omega(p)}{\omega(0)} = \left[\frac{c(p)}{c(0)}\right]^{-3\gamma_\parallel}, \quad (9)$$

where c is the lattice parameter associated with the interlayer separation. $\gamma_\parallel$ has been discussed by Hanfland *et al.* [18] following the above scaling relation proposed by Zallen [38] to conclude that, due to its larger value, the anharmonicity of the $E_{2g}(1)$ mode is greater than that of the high-frequency $E_{2g}(2)$ one. We notice that instead of an average value for this linear Grüneisen parameter, as reported by Hanfland *et al.* [18], we evaluate a number of $\gamma_\parallel$-p values for a better view of the dependence of anharmonicity on pressure.

A final remark concerning our modeling is related with the equivalence of uniaxial and hydrostatic stresses. We have not found any meaningful difference in the interlayer spacing obtained under the same stress conditions either hydrostatic or uniaxial along the c axis. It should therefore be understood that the blue-shift experienced by this frequency is a pure effect of the enhancement of vdW interactions as the spacing between graphene layers decreases. This can be of interest in the discussion of the contributions (covalent and vdW) to the frequencies of other in-plane modes, as the $E_{2g}(2)$ one recently analyzed by Sun *et al.* [28], who proposed a partition of the Grüneisen parameter into in-plane and out-of-plane contributions.

IV. FREQUENCY EVALUATION AND COMPARISON WITH EXPERIMENT

Evaluation of the anharmonicity of a vibrational mode involves not only the knowledge of the energy around the energy minimum, but also its dependence on displacements far from the equilibrium. It becomes necessary to examine whether a simple analytical expression as the Morse function fits in a reliable manner, the one-dimensional potential landscape of graphite between the AAA and AB′A maxima (see Fig. 1). We have analyzed the quality of Morse fittings to the $E_{2g}(1)$ energetic profiles calculated in Ref. [16] for a number of interlayer distances, including the computed [16] and experimental [39] zero-pressure c values 6.43 and 6.71 Å, respectively. Reduced χ-square values are in the range 10^{-8}–10^{-9}, the residuals are equally distributed between negative and positive values with sums approximately 10^{-8} in all cases, four orders of magnitude less than the increment of the calculated DFT values. These results corroborate that Morse potentials describe accurately the energetics of the $E_{2g}(1)$ vibrational mode. Selected examples of the Morse fittings for different interlayer distances are shown in Fig. 5.

We subsequently used the Morse fitting parameters to obtain harmonic frequencies for all interlayer spacings. The results are collected in Table I. We notice that our computed harmonic frequency at the zero-pressure equilibrium geometry (50 cm^{-1}) is in good agreement with the experimental value of Hanfland *et al.* (44 cm^{-1}) [18]. Most of previous reported experimental and calculated values for the frequency of this mode lie in the range 40–50 cm^{-1} [17,21,23,24,40–42].

Now, we are in conditions for quantifying the anharmonicity of the graphite frictional mode. The anharmonic effect is

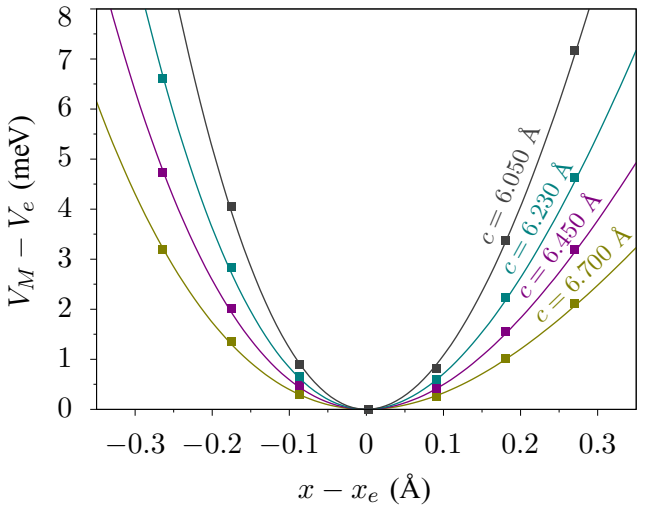

FIG. 5. Morse potential fittings for the calculated data at different values of the lattice parameter c. Notice that the smaller the value of c, the more harmonic each curve becomes.

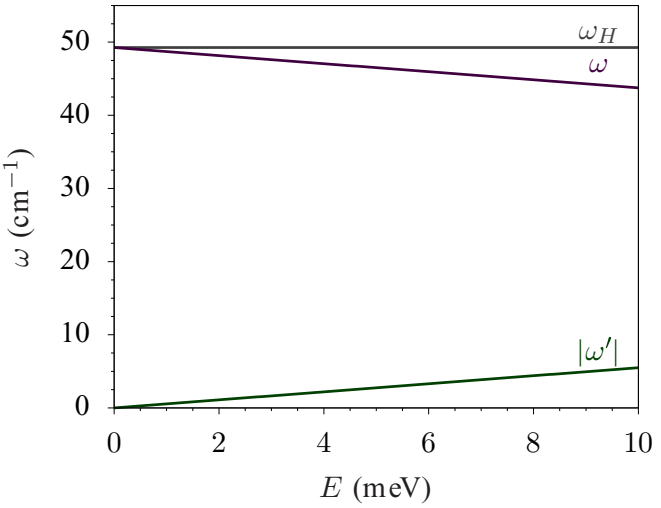

FIG. 6. Variation of total ω, harmonic ω_H, and anharmonic contributions ω', with the available vibrational energy E at zero pressure.

due to the softening experienced by a normal vibration mode due to a modification of the interaction distance. In the classical picture of the nonlinear oscillations [see Eq. (7)], this effect depends both on the available energy of the system (amplitude of the oscillation) and on the harmonic frequency ω_H, which is constant at a given pressure. An increase in energy produces a decrease in the vibrational frequency due to the fact that the system is in a higher vibrational state. To illustrate this contribution, we show in Fig. 6 how the frequency ω is reduced as the available energy increases at zero pressure. In particular, we can see that the potential asymmetry leads to a red-shift of 2 cm^{-1} when the harmonic amplitude of the vibration is around 0.2 Å (the available energy is around 2 meV), and decreases linearly up to -6 cm^{-1} when the available energy reaches 10 meV. Thus, we can conclude that the contribution of anharmonicity to the actual frequency of the $E_{2g}(1)$ mode cannot be neglected. By quantifying the oscillation width, we have another perspective of the importance of anharmonic effects. For a harmonic vibration, the oscillation width is simply $2A$. It amounts a value of 0.350 Å when the available vibrational energy is 2 meV. If the potential asymmetry is taken into account, the oscillation width goes up to 0.385 Å. Such an almost 10% increasing in the vibrational elongation is large enough to be taken into account in the analysis and evaluation of graphite properties.

TABLE I. Calculated Morse fitting parameters, and harmonic frequencies for selected interlayer distances.

$c/2$ (Å)	N (Å^{-1})	M (eV)	x_e (Å)	ω_H (cm^{-1})
3.3500	0.91810	0.04265	2.84208	41.81
3.2500	0.88189	0.06414	2.84200	49.25
3.2050	0.85967	0.07793	2.84205	52.92
3.1600	0.83405	0.09541	2.84203	56.81
3.1150	0.80186	0.11870	2.84203	60.92
3.0700	0.76087	0.15140	2.84204	65.29
3.0250	0.71026	0.19935	2.84197	69.93
2.9125	0.56217	0.43618	2.83832	81.37
2.8000	0.50181	0.53746	2.83922	91.67

The available vibrational energy is related to the temperature of the graphite sample. However, a rigorous relationship is not straightforward if we look for an accurate estimation of the effect of T on the anharmonic contribution to the frequency. Phonon-phonon and phonon-electron interactions in graphite are important [22] and could lead to a complex temperature-energy dependence. This is out of the scope of our study. Nevertheless, we can give an estimation of the available vibrational energy at a given temperature by considering the vibrational partition function within the harmonic approximation. For example, at room temperature the estimated value of the vibrational energy is about 3 meV/atom, which leads to an anharmonic contribution of -2.6 cm^{-1}, higher in absolute value but of the order of magnitude of the plotted values reported by Bonini *et al.* [22] for the $E_{2g}(2)$ high-frequency mode. In the classic limit, energy and temperature are linearly related and the decreasing trend of the frequency as the available energy increases would indicate the same behavior when temperature is considered. This suggests that the intrinsic anharmonic effect leads to a decreasing in the fictional forces of graphite as temperature increases.

Concerning the effect of pressure, the expected behavior of an increasing harmonic frequency as the interlayer separation decreases or the pressure/uniaxial stress increases was obtained. This result is also in agreement with an intuitive view of friction, a reduction on the graphene interlayer distance means that the interaction between layers becomes stronger. As the graphene layers approach each other, the springs are compressed making more difficult the relative displacement of the layers along the x axis. Specifically, we illustrate in Fig. 7 (left) how the same trend is followed by the actual calculated harmonic frequencies (Table I) and the results from the four-spring model [Eq. (2)] when arbitrary values (to be in the same scale) for the spring constant and the mass ($k_s = 1$, $m = 1$) is used. Results nicely reveal that the trends are comparable in a qualitative way.

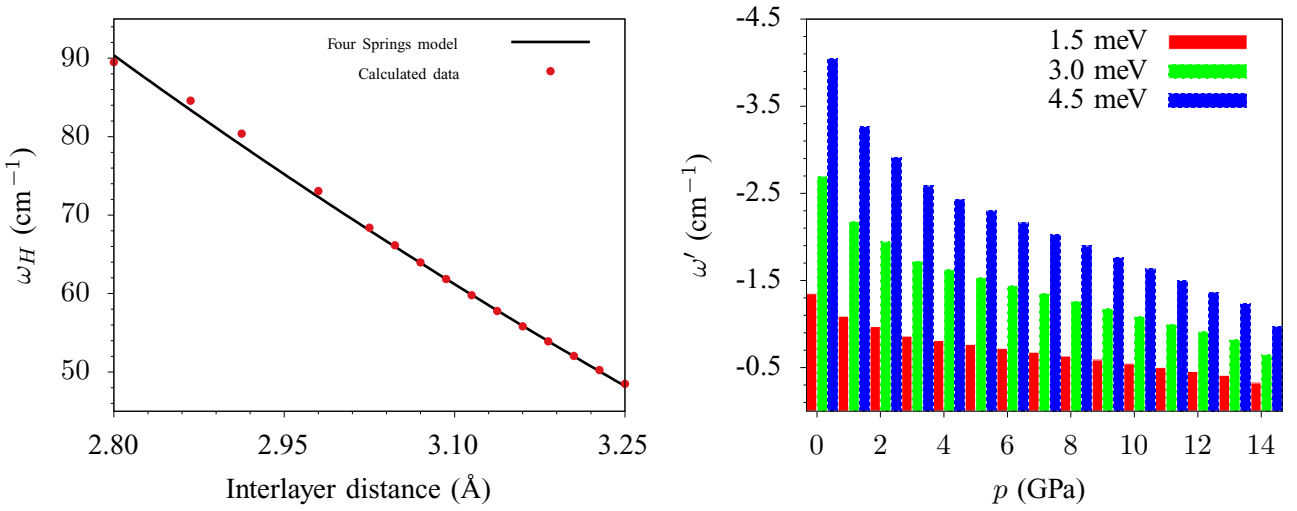

FIG. 7. Variation of harmonic frequencies with interlayer spacing according to our calculations and the four-springs model trend (left), and variation of the anharmonic contribution with pressure for the energies 1.5, 3.0, and 4.5 meV (right).

If we look for the effect of pressure on the anharmonic contribution, then Fig. 7 (right) has to be examined. Regardless the available energy of the system, continuous reduction of the anharmonicity is found as pressure is applied. This is also in agreement with the changes observed in the shape of the energetic profiles of Fig. 5 as the c parameter decreases, where the potential asymmetry is reduced. As expected, the vibrational frequency of the $E_{2g}(1)$ mode (Fig. 8) increases as a consequence of the enhancement of π-type interactions between graphene layers upon compression. In addition, the progressive approaching of the bond charge densities perpendicular to the graphene sheets enhances repulsive interactions that are greater and more effective in the AAA and AB′A configurations than in the minimum energy ABA configuration (see discussion of Fig. 2). A stiffer potential

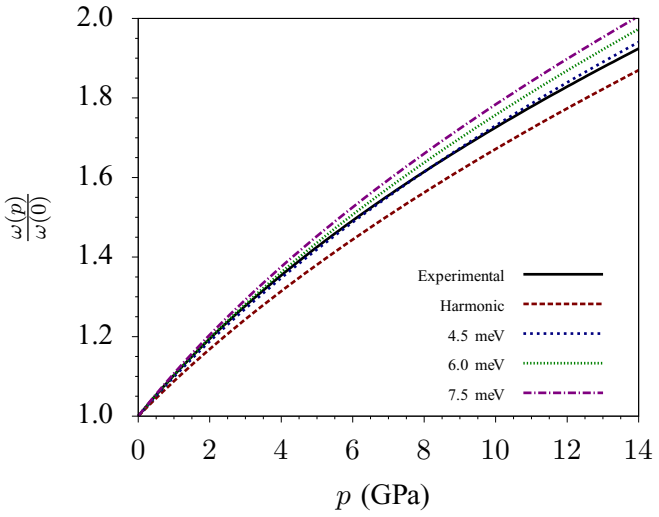

FIG. 8. Variation of the normalized frequencies with pressure according to our calculations at different energies and experimental values. Pressure and c are also related through a Murnaghan-type equation (*see* Ref. [18]).

results as pressure increases (see also Ref. [16]) and, therefore, a higher vibrational frequency is obtained.

It is to be noted that the effect of pressure on the actual frequency is about one order of magnitude larger than and opposite to the effect of anharmonicity. The resulting normalized frequency (harmonic plus anharmonic perturbation) for available energies between 0 and 7.5 meV is plotted in Fig. 8 up to 14 GPa. Comparison with the fit to experimental data of Hanfland *et al.* [18] reveals that the pure harmonic contribution is unable to account for the pressure dependence of the frequency of this mode. Only when the anharmonic contribution is taken into account, a faithful description of the experimental data is obtained. The fitting parameters δ_0 and δ' obtained for an available energy of 4.5 meV [0.104(6) GPa^{-1} and 0.47(5), respectively], are in excellent agreement to those derived from the experiment [18]: $\delta_0 = 0.110(8)$ GPa^{-1} and $\delta' = 0.43(3)$. It must be stressed that the available energy has to be understood as an average thermal energy available for the system.

Let us finalize our analysis by comparing calculated and experimental linear Grüneisen parameters ($\gamma_\parallel$). This is an excellent descriptor of the anharmonicity of the $E_{2g}(1)$ mode and how the blue-shift in frequency is linked to the reduction of the lattice parameter c as pressure is applied. It is also to be emphasized that changes in Grüneisen-type parameters unveil changes in the bond strength involved in the specific vibrational mode. By combination of Eqs. (8) and (9), we can evaluate the pressure dependence of $\gamma_\parallel$ using δ_0 and δ' obtained under both harmonic and anharmonic scenarios. In order to compare with available experimental data, average $\overline{\gamma_\parallel}$ values were also calculated. The overall results are displayed in Fig. 9.

Inspection of this figure clearly illustrates two key aspects on the anharmonic behavior of the $E_{2g}(1)$ mode. By analyzing calculated average $\overline{\gamma_\parallel}$ values, it can be seen that only those considering anharmonic contributions lie within the confidence interval of the experimental value reported by Hanfland *et al.* [18], and this reinforces the idea that a realistic description of

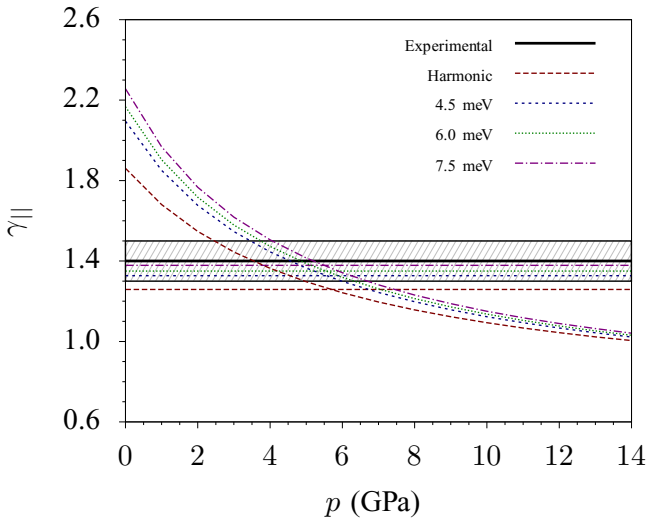

FIG. 9. Variation of the linear Grüneisen parameter with pressure according to our calculations for different available energies. Average calculated and experimental values are also displayed (dashed region accounts for the experimental confidence interval, see Ref. [18]).

graphite physical properties requires a good quantification of anharmonic effects. But Fig. 9 also evidences a strong variation of $\gamma_{\|}$ with pressure, in clear analogy with the requirement for introducing the so-called Anderson-Grüneisen parameter in equation-of-state theory [43]. In particular, it is shown that $\gamma_{\|}$ roughly varies from 2.0 at zero pressure to 1 at 14 GPa. In addition, the asymptotic convergence of $\gamma_{\|}$ seems to reinforce the idea that anharmonicity decreases with increasing pressure, at least in such an anharmonic mode. In any case, the whole trend reveals that the actual anharmonic behavior of $E_{2g}(1)$ is largely influenced by pressure or stress, so the use of an average Grüneisen parameter will never provide an accurate description of graphite properties along the c axis.

Changes in Grüneisen parameters of the order of 1 have been typically associated with indications of interaction changes, i.e., from intermolecular to intramolecular interactions or changes from ionic to covalent bonds [38,44]. In the case of graphite, the decreasing of $\gamma_{\|}$ can be correlated with the progressive emergence of directional charge bonding interactions between sheets. As pressure increases, graphene layers approach, and bond charge densities perpendicular to the plane begin to interact, increasing their directional character as a consequence of the reduction of their interaction volume. Although, according to Isea [45], it is not until 2.0 Å when two C atoms start to show a covalent bond, our analysis indicates that the nature of the interactions is changing in that sense. In fact, covalent interlayer bonding in bilayer graphene was already reported by Andres *et al.* for interlayer separations around 1.5 Å in the AA stacking [26], thus confirming the change in the nature of the interactions involved in the $E_{2g}(1)$ mode as pressure increases.

V. CONCLUSIONS

By detailed exploration of relative rigid-layer displacements of graphite layers, we have detected the existence of two different stackings (AAA and AB′A) around the ABA equilibrium configuration. DFT-based calculations reveal that whereas ABA is the absolute minimum of the energy surface, AAA and AB′A are two maxima with different energies. In consequence, the $E_{2g}(1)$ mode associated with this shearlike displacement must evidence anharmonicity. In fact, the whole potential energy surface discloses that the anharmonicity is anisotropic with specific displacement directions showing harmonicity.

The energetic profiles of the $E_{2g}(1)$ mode at different uniaxial or hydrostatic stress conditions can be accurately described with simple Morse-type functions that can be manipulated following a perturbative treatment to account for a partition of the vibrational frequency in harmonic and anharmonic contributions. As no meaningful changes in intralayer C-C distances are found along the vibrational coordinate, our results provide a source of information of pure interlayer interactions that can be useful in the analysis of other vibrational modes where both interlayer and intralayer effects are simultaneously present [28].

The anharmonic contribution to the $E_{2g}(1)$ frequency at zero pressure depends on the amplitude of the vibration and can be evaluated by introducing an available energy to the system. In the range 0–10 meV, the reduction of the actual frequency can be as large as 6 cm^{-1} if anharmonicity is taken into account. On the other hand, pressure increases the value of the frequency and decreases the anharmonic contribution. Both effects are a consequence of the enhancement of interlayer interactions due to the approaching of graphene sheets as pressure is applied. We have quantified the increasing of the harmonic frequency (also reproduced qualitatively with a simple four-spring model) and the decreasing of the anharmonicity, still greater than 1–2 cm^{-1} even at 14 GPa. When comparing with experimental ω-p pressure data [18], we found a very good agreement only when anharmonicity is included in our calculations. The best fit is obtained when the vibrational energy of the $E_{2g}(1)$ mode is 4.5 meV. Our results indicate that frictional forces between graphene sheets in graphite decrease as temperature increases (the available vibrational energy is higher) and increase as pressure is applied. Details of the calculations of frictional forces and coefficients using our 3LG slab model were previously reported in a separate study [16].

The anharmonicity of this mode is well characterized by the linear c-like Grüneisen parameter $\gamma_{\|}$. We have evaluated its dependence on pressure adding information to existing experimental data that only reported an average value [18]. We observed again that only average $\overline{\gamma_{\|}}$ computed with anharmonic curves are able to provide values within the confidence interval of the experimental value. However, we have shown that this average value must be substituted by the $\gamma_{\|}(p)$ curve since a noticeable decreasing of this linear Grüneisen parameter is obtained in the 0–14 GPa range. Both the asymptotic value reached by all the curves close to a value of 1 and the difference between the zero pressure and the 14-GPa value of $\gamma_{\|}$ are worth to be remarked: the former because the asymptotic value indicates the decreasing of the anharmonicity towards a harmonic behavior of this mode and the latter because it is related to a change in the nature of the chemical interactions between graphene layers, as previously illustrated in few-layer graphene systems [26].

ACKNOWLEDGMENT

Financial support from the Government of Principado de Asturias, (Spain) (Project No. GRUPIN14-049), the Spanish Ministerio de Economia y Competitividad and FEDER programs under Projects No. CTQ2012-35899-C02 and No. CTQ2015-67755-C2, and the Spanish MALTA-Consolider Team under Project No. MAT2015-71070-REDC are gratefully acknowledged.

[1] R. H. Savage, J. Appl. Phys. **19**, 1 (1948).
[2] B. Bhushan, *Introduction to Tribology* (Wiley, New York, 2002).
[3] B. Bhushan, J. N. Israelachvili, and U. Landman, Nature (London) **374**, 607 (1995).
[4] Z. Deng, A. Smolyanitsky, L. Qunyang, X-Q. Feng, and R. J. Cannara, Nature Mater. **11**, 1032 (2012).
[5] Y. Mo, K. Turner, and I. Szlufarska, Nature (London) **457**, 1116 (2009).
[6] C. M. Mate, G. M. McClelland, R. Erlandsson, and S. Chiang, Phys. Rev. Lett. **59**, 1942 (1987).
[7] C. G. Lee, Q. Li, W. Kalb, X.-Z. Liu, H. Berger, R. W. Carpick, and J. Hone, Science **328**, 76 (2010).
[8] T. Filleter, J. L. McChesney, A. Bostwick, E. Rotenberg, K. V. Emtsev, T. Seyller, K. Horn, and R. Bennewitz, Phys. Rev. Lett. **102**, 086102 (2009).
[9] A. L. Kitt, Z. Qi, S. Remi, H. S. Park, A. K. Swan, and B. B. Goldberg, Nano Lett. **13**, 2605 (2013).
[10] Z. Liu, J. Yang, F. Grey, J. Z. Liu, Y. Liu, Y. Wang, Y. Yang, Y. Cheng, and Q. Zheng, Phys. Rev. Lett. **108**, 205503 (2012).
[11] A. Socoliuc, R. Bennewitz, E. Gnecco, and E. Meyer, Phys. Rev. Lett. **92**, 134301 (2004).
[12] A. Smolyanitsky and J. P. Killgore, Phys. Rev. B **86**, 125432 (2012).
[13] M. Hirano and K. Shinjo, Phys. Rev. B **41**, 11837 (1990).
[14] M. Dienwiebel, G. S. Verhoeven, N. Pradeep, J. W. M. Frenken, J. A. Heimberg, and H. W. Zandbergen, Phys. Rev. Lett. **92**, 126101 (2004).
[15] Y. Guo, W. Guo, and C. Chen, Phys. Rev. B **76**, 155429 (2007).
[16] D. Abbasi-Pérez, J. M. Menéndez, J. M. Recio, A. Otero-de-la-Roza, E. del Corro, M. Taravillo, V. G. Baonza, and M. Marqués, Phys. Rev. B **90**, 054105 (2014).
[17] D. P. Di Vincenzo, E. J. Mele, and N. A. W. Holzwarth, Phys. Rev. B **27**, 2458 (1983).
[18] M. Hanfland, H. Beister, and K. Syassen, Phys. Rev. B **39**, 12598 (1989).
[19] R. Kostić, M. Mirić, T. Radić, M. Radović, R. Gajić, and Z. V. Popović, Acta Polon. **116**, 718 (2009).
[20] R. J. Nemanich, G. Lucovsky, and S. A. Solin, Proc. Int. Conf. Lattice Dynamics 619, (1977).
[21] M. S. Dresselhaus, G. Dresselhaus, P. C. Eklund, and D. D. L. Chung, Mater. Sci. Eng. **31**, 141 (1977).
[22] N. Bonini, M. Lazzeri, N. Marzari, and F. Mauri, Phys. Rev. Lett. **99**, 176802 (2007).
[23] R. Al-Jishi and G. Dresselhaus, Phys. Rev. B **26**, 4514 (1982).
[24] C. S. G. Cousins and M. I. Heggie, Phys. Rev. B **67**, 024109 (2003).
[25] J.-C. Charlier, X. Gonze, and J.-P. Michenaud, Phys. Rev. B **43**, 4579 (1991).
[26] P. L. de Andres, R. Ramírez, and J. A. Vergés, Phys. Rev. B **77**, 045403 (2008).
[27] M. Birowska, K. Milowska, and J. A. Majewski, Acta Phys. Polon. A **120**, 845 (2011).
[28] Y. W. Sun, D. Holec, and D. J. Dunstan, Phys. Rev. B **92**, 094108 (2015).
[29] C. R. C. Rêgo, L. N. Oliveira, P. Tereshchuk, and J. L. F. Da Silva, J. Phys.: Condens. Matter **27**, 415502 (2015).
[30] L. Paulatto, F. Mauri, and M. Lazzeri, Phys. Rev. B **87**, 214303 (2013).
[31] J. P. Perdew, K. Burke, and M. Ernzerhof, Phys. Rev. Lett. **77**, 3865 (1996).
[32] G. Kresse and J. Furthmuller, Phys. Rev. B **54**, 11169 (1996).
[33] H. J. Monkhorst and J. D. Pack, Phys. Rev. B **13**, 5188 (1976).
[34] S. Grimme, J. Comput. Chem. **27**, 1787 (2006).
[35] T. Bučko, J. Hafner, S. Lebégue, and J. G. Ángyán, J. Phys. Chem. A **114**, 11814 (2010).
[36] L. N. Kantorovich, http://www.cmmp.ucl.ac.uk/lev/codes/lev00/index.html
[37] L. D. Landau and E. M. Lifshitz, *Mechanics*, Vol. 1 of A Course of Theoretical Physics, 3rd ed. (Pergamon, Oxford, 1976).
[38] R. Zallen, Phys. Rev. B **9**, 4485 (1974).
[39] M. Mohr, J. Maultzsch, E. Dobardzic, S. Reich, I. Milosevic, M. Damnjanovic, A. Bosak, M. Krisch, and C. Thomsen, Phys. Rev. B **76**, 035439 (2007).
[40] R. J. Nemanich and S. A. Solin, Phys. Rev. B **20**, 392 (1979).
[41] Y. Wang, D. C. Alsmeyer, and R. L. McCreery, Chem. Mater. **2**, 557 (1990).
[42] S. Reich and C. Thomsen, Philos. Trans. R. Soc. London A **362**, 2271 (2004).
[43] O. L. Anderson, *Equations of State of Solids for Geophysics and Ceramic Science*, Oxford Monographs on Geology and Geophysics, Vol. 31 (Oxford University Press, New York, 1995).
[44] W. F. Sherman, J. Phys. C: Solid State Phys. **13**, 4601 (1980).
[45] R. Isea, J. Mol. Struct. (THEOCHEM) **540**, 131 (2001).